Available online at www.sciencedirect.com
SCIENCE DIRECT®
ELSEVIER
Earth and Planetary Science Letters 6927 (2003) 1–14
EPSL
www.elsevier.com/locate/epsl

Redox state, microstructure and viscosity of a partially crystallized basalt melt

M. Ali Bouhifd [a,b], Pascal Richet [a,*], Pascale Besson [b], Mathieu Roskosz [a,c], Jannick Ingrin [d]

[a] *Physique des Minéraux et des Magmas, UMR 7047, Institut de Physique du Globe de Paris 4, Place Jussieu, 75252 Paris Cedex 05, France*
[b] *Laboratoire des Géomatériaux, UMR 7046, Institut de Physique du Globe de Paris 4, Place Jussieu, 75252 Paris Cedex 05, France*
[c] *CRPG, CNRS UPR 2300, 15 Rue Notre-dame des Pauvres, BP 20, 54501 Vandœuvre-lès-Nancy Cedex, France*
[d] *Laboratoire de Minéralogie, UMR 5563, 39 allées Jules Guesde, 31000 Toulouse, France*

Received 18 July 2003; received in revised form 6 October 2003; accepted 31 October 2003

Abstract

As measured in air above the glass transition range, the viscosity of an alkali basalt increases markedly with time by about two orders of magnitude in 12 h. This effect is essentially physical and due to the presence of microcrystals although partial crystallization of the melt into spinel and an SiO_2-poor pyroxene leads to a considerable enrichment in silica of the residual liquid. Partial crystallization depends strongly on the initial redox state of samples in that the presence of ferrous iron is required for spinel crystals to form and for pyroxene to nucleate and grow around them. Other measurements show that the viscosity of the crystal-free liquid decreases slightly with increasing ratios $r = Fe^{2+}/\Sigma Fe$ because the differences between samples with $r = 0.16$ and 0.83 amount to about 1.5 and 0.3 log-units at 950 and 1400 K, respectively. Comparisons of the viscosities of the residual liquid matrix and of the initially crystal-free basalt show that physical effects caused by the presence of microcrystals begin to be observed at a low crystal fraction of 5 vol%. Finally, a model of viscosity calculation is developed for the melts which reproduces all data obtained in this work to better than 10%.

Keywords: basalt; viscosity; crystallization; redox

1. Introduction

At all scales, the effective viscosity of a magmatic suspension is an essential parameter influencing petrological and volcanological processes, from rates of crystal growth and gravitative settling to the buoyant rise of bubbles and the mode of volcanic eruption. Although basaltic melts are especially important in this respect, their viscosities have mostly been measured for homogeneous liquids at temperatures higher than 1270 K [1,2]. Because knowledge of viscosity is actually needed at subliquidus temperatures, measurements near the glass transition are needed to complement the high-temperature data. As far as we are aware,

* Corresponding author. Tel.: +33-1-44-27-49-38; Fax. +33-1-44-27-24-87.
E-mail address: richet@ipgp.jussieu.fr (P. Richet).

0012-821X/03/$ – see front matter © 2003 Published by Elsevier B.V.
doi:10.1016/S0012-821X(03)00641-1

however, these measurements are scarce for basalts or related melts. Examples are studies by Cukierman and Uhlmann [3], made between 873 and 973 K on a lunar composition, by Exnar and Voldan [4], and Giordano and Dingwell [5] on an Etna basalt between 1000 and 1820 K.

A primary aim of our study has been to determine the viscosity of a basalt melt at high and low temperatures in order to make interpolations possible in the petrologically relevant temperature intervals. For iron-rich materials such as molten basalts, an important concern is the oxidation state of samples in view of the significant effect of the redox state on viscosity that has long been demonstrated [3,6–13]. As a matter of fact, the 10-fold viscosity increase with time observed by Neuville et al. [14] for an andesite liquid above the glass transition range was tentatively ascribed to oxidation of ferric into ferrous iron during the experiments.

In this contribution, we report new viscosity experiments on partially crystallized basalt samples with different redox state ($Fe^{2+}/\Sigma Fe$ ratios (r) ranging from 0.16 to 0.83). These experiments allow one to quantify the effects of both $Fe^{2+}/\Sigma Fe$ and the degree of crystallization on the viscosity of partially crystallized melts. The time dependence of the viscosity was actually due to partial crystallization, whose rate was strongly dependent on the initial redox state of the sample. This complication has in fact the advantage of allowing the influence of partial crystallization on the rheology of molten basalt to be determined. However, our viscosity measurements made on three samples with different redox state then demonstrated that the kinetics of redox reactions are much too slow below about 1000 K to cause significant viscosity changes.

Another important goal of our work has thus been to separate the physical effects due to the presence of crystals from the chemical effects induced by the changing composition of the melt. For this purpose, we have used analytical transmission electron microscopy (ATEM) to identify the crystallizing phases and analyze their composition and that of the residual glass matrix. We have also measured the viscosities of five synthetic melts simulating the residual melt phase during basalt crystallization for crystal fractions ranging from about 5 to 60 vol%. Finally, we have examined basalt fibers subjected to the same heat treatments to detect a possible influence of surface conditions on partial crystallization.

This study thus complements the observations made under similar high-viscosity conditions on simple congruently melting systems [15,16] or at higher temperatures on complex compositions (e.g. [17–19]). While the latter measurements are difficult to interpret because of rapid changes in the crystal fraction, the present measurements deal with phases crystallizing when a glass is heated above the glass transition. These phases generally differ from those forming at higher temperatures when a magma is cooled. This is not an important drawback, however, for our purpose is to determine the physical and chemical effects at work under conditions controlled as tightly as possible. In other words, we are more interested in establishing procedures with which these effects can be accounted for in a general way rather than in determining the rheology of a particular basalt melt under some specific conditions.

2. Experimental methods

2.1. Starting materials

An alkali basalt from Stein Frentz (Germany), dubbed SFB, was chosen as the starting material. To compare the viscosities of this basalt and those simulating the residual glassy matrix after different crystallization stages, we synthesized the five compositions listed in Table 1. These compositions were prepared from oxide and carbonate mixes through repeated cycles of grinding and fusion at around 1800 K. The chemical compositions of the glasses were checked by electron microprobe analyses (Table 1). They are in very good agreement with the nominal values [20]. The vitreous nature of the quenched products was checked by X-ray diffraction and transmission electron microscopy (TEM). In Table 1 is included the room-temperature density of the glasses as measured with an Archimedean method, toluene used as the immersion liquid. We also

Table 1
Chemical composition (wt%)[a] of Stein Frentz basalt (SFB) and the glassy matrix compositions SFB5, SFB10, SFB20, SFB40 and SFB60

	SFB	SFB5	SFB10	SFB20	SFB40	SFB60[b]
SiO_2	46.58 (18)	48.23 (20)	49.34 (83)	51.58 (47)	58.97 (22)	74.84 (40)
Al_2O_3	13.28 (15)	13.10 (09)	12.80 (14)	12.12 (14)	9.86 (06)	4.24 (06)
Na_2O	5.60 (20)	5.63 (12)	6.10 (16)	6.48 (30)	8.99 (17)	11.34 (20)
K_2O	1.38 (07)	1.45 (03)	1.52 (06)	1.76 (04)	2.34 (05)	3.39 (08)
FeO	11.20 (20)	10.23 (22)	9.86 (33)	8.93 (27)	7.24 (13)	1.19 (05)
CaO	10.00 (10)	10.01 (08)	9.62 (17)	9.24 (19)	5.33 (12)	1.96 (08)
MgO	9.15 (08)	8.91 (07)	8.10 (16)	7.24 (11)	4.56 (06)	1.98 (04)
TiO_2	2.45 (05)	2.32 (07)	2.12 (08)	1.51 (05)	1.58 (09)	0.50 (05)
Total	99.64	99.88	99.46	98.86	98.87	99.44
ρ[c]	2.862	2.775	2.773	2.740	2.595	2.424
$Fe^{2+}/\Sigma Fe$[d]	0.43	0.29	0.26	0.26	0.33	

[a] Average of 10 analyses made with a Camebax electron microprobe, uncertainties on the last digits given by the numbers in parentheses.
[b] The iron content is too low to get a Mössbauer spectrum.
[c] Room-temperature Archimedean density (g/cm^3) of the glasses.
[d] The ratio $Fe^{2+}/\Sigma Fe$ is determined either from wet chemical analyses for SFB glass or by Mössbauer spectroscopy for SFB5, SFB10, SFB20 and SFB40.

list the redox ratio as determined by either wet chemical analyses or by Mössbauer spectroscopy (mesurements kindly performed by B.O. Mysen, Geophysical Laboratory, Carnegie Institution of Washington).

2.2. Viscosity measurements

The creep apparatus described by Neuville and Richet [21] was used to measure viscosities from the observed deformation rate as a function of the applied stress:

$$\eta = \sigma/3(\mathrm{d}\ln l/\mathrm{d}t) \quad (1)$$

where l is the length of the sample, t the time and σ the stress. Measurements on NIST standard glasses indicate that the results are accurate to better than 0.04 log-unit. Stresses and strain rates were typically in the ranges 10–10^4 bar and 10^{-3}–10^{-5} s^{-1}, respectively. The reported data are the average of about 10 measurements made at different stresses. The standard deviations from the mean are generally smaller than 0.02 log Pa s, which indicates that, unless otherwise noted, the reported viscosities are Newtonian. Samples were cylinders initially from 3 to 6 mm in diameter, with a height ranging from 6 to 12 mm. Their opposite faces were ground and polished to achieve parallelism to within a few μm. The time required to heat the samples from room temperature to the temperature of the experiment and then to achieve thermal stability and isothermal conditions to within ±0.1 K was about 1 h.

At high fluidity, the viscosity was measured with the rotating coaxial cylinder setup described by Vignesoult and Thelohan [22], which was calibrated with the NIST 710 standard glass. Platinum and molybdenum crucibles and bobs were used for measurements in air and nitrogen, respectively. Wet chemical analyses of the iron redox ratio were made before and after viscometry.

2.3. TEM observations

The observations by TEM were made with a Topcon 002B microscope (LaB_6 gun, 200 keV), and the chemical analyses with a TN3ss.N energy-dispersive X-ray spectrometer attached to the microscope and equipped with an ultra-thin window suitable for light-element analysis. For spectrum analysis, the method developed by Van Capellen is used [23–25]. For the viscosity samples, the observations were made directly on very fine powders ground into ethanol and deposited on a carbon film mesh. For glass fibers, the samples were prepared from a set of five to 10 fibers

glued with epoxy across the 400 μm central hole of copper grids with a single aperture, argon ion thinned at 5 kV for a few hours under an angle of 15°, and finally carbon-coated on both sides.

2.4. Determination of crystal fractions

The crystalline fractions developed during viscosity measurements were evaluated by ATEM. A window of 500 nm × 250 nm across the observed area was selected for determining the modal composition. Several areas in the same sample were selected in order to have more precise crystal fractions. In this way we estimate the errors as ±2 vol% and ±5 vol% for crystal fractions around 5 and 50 vol%, respectively. As an indirect check of these crystal fractions, the chemical composition of the residual glass was determined by ATEM. It agreed well with that calculated after taking into account the analyzed composition of the crystals and their estimated volume fractions.

3. Results

3.1. Viscosity and density of SFB (r = 0.43)

For measurements made between 10^9 and 10^{12} Pa s, the major feature is the important increase

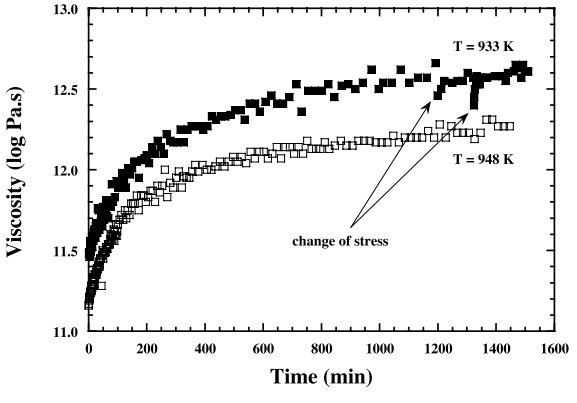

Fig. 1. Time dependence of the viscosity of partially crystallized SFB melts with $r = 0.43$ at 933 and 948 K. Note the Newtonian nature of the viscosity as indicated by the rapid relaxation to the initial value after stress changes successively made from 65 to 208 and from 208 to 810 bar during the 933 K experiment.

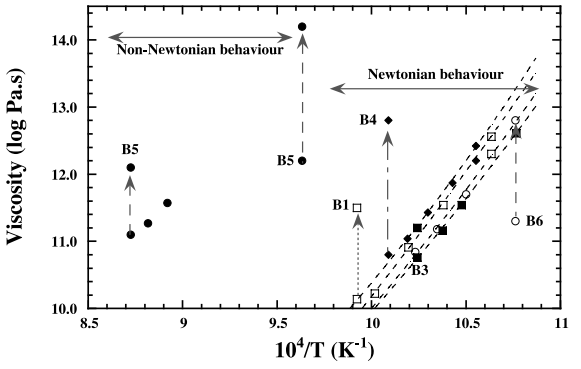

Fig. 2. Viscosity of partially crystallized basalt in the range 10^{10}–10^{14} Pa s. The arrows indicate the viscosity increases observed during the experiments (Table 2). All samples were prepared in the same way (see text), except sample B5, which was annealed in air at 973 K for 24 h prior to the measurements.

of the viscosity of our basalt with time at constant temperature (Fig. 1). After a typical 10-fold increase in about 10 h, the viscosity then leveled off and remained Newtonian, as shown in Fig. 1, by the insensitivity of the measured values to stress variations. A time dependence was also observed for the viscosity of an andesite melt by Neuville et al. [14], who ascribed it to partial oxidation of the sample during the measurements. However, wet chemical analyses did not indicate changes in the redox ratio of our partially crystallized basalt samples after experiments. Even if the measured redox is that of the bulk sample, it must be close to the redox of residual melt as the crystal fractions are lower than 5 vol% for all these samples. In contrast, partial crystallization of the samples during the measurements was clearly revealed by X-ray diffraction experiments.

The viscosities measured as rapidly as possible for a series of six samples of SFB ($r = 0.43$) are plotted in Fig. 2 and listed in Table 2, where the first and the limiting measured viscosity are included. These measurements show that the viscosity of partially crystallized basalt strongly depends on the thermal history of the samples and thus on the duration of the experiments. For instance, the viscosity of sample B1 is about one order of magnitude higher than that of B2 (see Table 2), which is related to the fact that the temperature of the first measurement was 998 and 953 K, respec-

Table 2
Viscosity (Pa s) of molten Stein Frentz basalt

#	T (K)	log η	Duration	#	T (K)	log η	Duration
B1	($\rho_i = 2.862$; $\rho_f = 2.959$)			B2	($\rho_i = 2.862$; $\rho_f = 2.852$)		
1	998.1	10.22	5	1	953	11.10	9
2	963.4	11.54	20	2	943	11.85	60
3	940.2	12.56	60				
4	980.7	10.91	21	B3	($\rho_i = 2.862$; $\rho_f = 2.858$)		
5	1008.0[a]	10.14		1	947.5[a]	12.22	
		11.77	25			12.61	780
				2	954.3	11.54	30
B6	($\rho_i = 2.862$; $\rho_f = 2.857$)			3	963.6	11.16	13
1	947.5[a]	12.22		4	976.3	10.76	
		12.42	1200			11.21	41
2	958.8	11.87	65				
3	970.9	11.43	36	B4[b]	($\rho_i = 2.861$; $\rho_f = 3.006$)		
4	981.3	11.04	24	1	929.1[a]	11.30	
5	991.0[a]	10.79				12.80	1335
		12.81	580	2	952.2	11.70	125
				3	966.3	11.18	11
				4	977.3[a]	10.84	
B5[b]	($\rho_i = 2.994$; $\rho_f = 3.038$)					11.05	30
Non-Newtonian viscosity (see text)							

Measurements reported in chronological order, duration of the experiments (min), and initial (ρ_i) and final (ρ_f) room-temperature density (g/cm^3).

[a] When the viscosity increased with time, the first and second values are the initial and final measurements, respectively.

[b] Samples B4 and B5 annealed at 973 K for 24 h in CO and in air, respectively, before viscometry.

tively, for these samples. Likewise, the viscosity of sample B5 is still higher (Fig. 2) because this sample was annealed in air at 973 K for 24 h before viscometry.

Macroscopically, the density of the materials is a sensitive probe of partial crystallization (Table 2). However, the density variations are not a monotonous function of the annealing time. When the temperature of the viscosity measurements was lower than 980 K the density decreased slightly (see samples B2, B3 and B6), whereas it increased markedly when the temperature exceeded 990 K (samples B1 and B4, Table 2).

3.2. *Effect of the redox state on viscosity and density of SFB*

In addition to time and temperature, the other important factor affecting both viscosity and partial crystallization is the iron redox ratio of the melt. Whereas the density of sample B5 increased by 5% after a 24-h annealing in air at 973 K, that of sample B4, from the same batch, did not change after an annealing of the same duration under a CO atmosphere and its viscosity was also similar to that of untreated samples (Fig. 2). To investigate the effect of the redox state on viscosity, three samples with different $Fe^{2+}/\Sigma Fe$ ratios were prepared. A ratio of 0.43 was obtained for a sample melted in air at 1800 K in a Pt crucible. This ratio was only 0.16 when oxygen was bubbled in the melt, and a value of 0.83 was obtained for another sample melted in a molybdenum crucible under a nitrogen atmosphere.

For these three samples, the viscosity was measured in air under the same conditions at about 930 and 950 K (Fig. 3). At each temperature the viscosity remained constant or increased only slightly with time for the reduced sample ($r = 0.83$), whereas it again increased by several orders of magnitude for the two others. These differences between the viscosity of the oxidized and reduced samples were the highest at the lowest temperatures. These observations suggest that

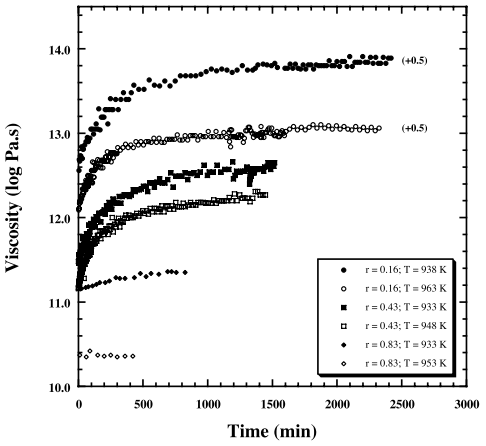

Fig. 3. Time dependence of the viscosity of partially crystallized basalt melts with various redox ratios at different temperatures. For clarity reasons, the two curves for oxidized sample ($r = 0.16$) have been displaced upwards by 0.5 log-units.

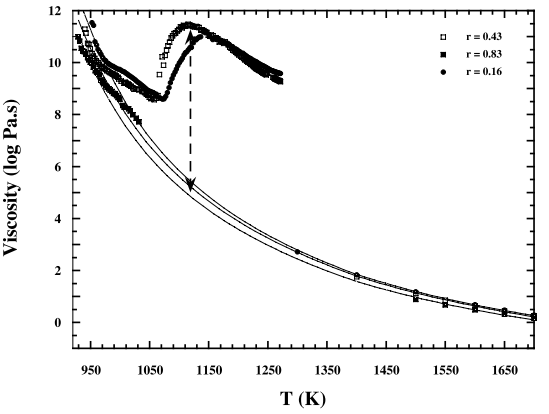

Fig. 5. Viscosities of basalt samples with different redox states measured isothermally at high temperatures with a Couette method and dynamically at 5 K/min above the glass transition. The six-order-of-magnitude effect of crystallization is indicated by the arrow that joins the curves representing the TVF equations of Table 3.

crystallization of basalt and the resulting increase of its viscosity with time at constant temperature are enhanced by high Fe^{3+} concentrations.

Another approach showing more clearly the effects of crystallization was followed to determine viscosities between 900 and 1100 K. These measurements were made dynamically at a constant heating rate of 5 K/min with a constant stress. As shown in Fig. 4 for a calcium magnesium silicate melt which does not crystallize during viscosity measurements, good agreement was ensured in this way with the static data, the differences between these two methods not exceeding 0.04 log-units for Newtonian viscosities. This agreement is a good test for the validity of this technique to measure directly the effect of crystallization during viscosity measurements over a wide range of temperatures.

The results obtained for the three basalt sam-

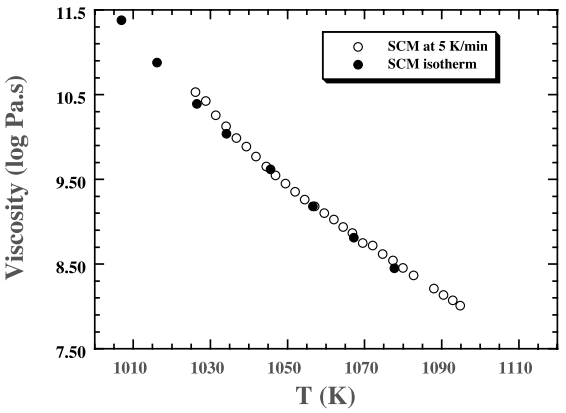

Fig. 4. Comparison between the viscosities measured isothermally (solid circles) and dynamically with a heating rate of 5 K/min (open circles) for a melt of composition 59.9 mol% SiO_2, 26.6 mol% CaO and 13.5 mol% MgO.

Table 3
Viscosities (Pa s)[a] of SFB melt for three redox ratios (r)

$r = 0.83$		$r = 0.43$		$r = 0.16$	
T (K)	log η	T (K)	log η	T (K)	log η
939.6	10.43	945.0	10.74	957.5	10.80
941.9	10.33	949.9	10.54	960.1	10.68
944.9	10.19	954.8	10.25	962.6	10.51
947.4	10.10	957.3	10.16	965.3	10.41
949.9	10.02	959.9	10.07	967.8	10.32
952.3	9.98	962.5	10.00	970.4	10.20
1500.0	0.88	1400.0	1.76	972.9	10.12
1550.0	0.67	1500.0	1.12	1400.0	1.83
1600.0	0.49	1550.0	0.86	1500.0	1.18
1650.0	0.32	1600.0	0.63	1600.0	0.68
1700.0	0.17	1650.0	0.43	1650.0	0.48
		1700.0	0.25	1700.0	0.29

[a] Viscosities not affected by sample crystallization (see text).

ples with different redox ratios are reported in Fig. 5 along with the values measured at superliquidus temperatures by Vignesoult and Thelohan [22] under either air or a nitrogen atmosphere.

No crystallization occured at about 950 K for the three sets of samples as checked by TEM observations. At these temperatures, the viscosity differences reflect the redox differences that we have already described. In conjunction with the high-temperature observations (Table 3), the data can be used to define the complete temperature–viscosity relationships indicated in Fig. 5 by solid lines. Empirically, these can be represented by Tammann–Vogel–Fulcher (TVF) equations:

$$\log \eta = A + B/(T - T_1) \quad (2)$$

where A, B and T_1 are adjustable parameters listed in Table 4 for the various redox ratios. At intermediate temperatures, the viscosity increases clearly demonstrate the marked differences in crystallization kinetics between the two oxidized and the reduced samples. Whereas the effect of crystallization on viscosity reached six orders of magnitude near 1150 K for the former, it was only a factor of 10 for the latter when the experiment had to be terminated at 1040 K because the values were becoming too low to be measured with our creep apparatus.

3.3. TEM observations

The TEM observations were made on samples taken either from the cylinders used for the low-viscosity measurements or from fibers with a redox ratio $Fe^{2+}/\Sigma Fe = 0.43$. First, no significant difference in microstructures was observed between both kinds of samples. Consistent with the rapid crystallization kinetics indicated by the viscosity measurements, this indicates that the influence of surface crystallization is small in comparison to homogeneous crystallization in the bulk. Within the resolution of the microscope, no crystals were detected in samples heated to temperatures lower than 950 K, except iron-rich crystals with a size of 15–50 nm that were forming under the electron beam. At 1000 K, the basalt formed microcrystals with a size of about 10 nm grouped in a heap of 120 nm (Fig. 6a). Two different phases were detected for samples heated at this temperature. These are close to spinel and pyroxene compositions, but the analyses of these phases were more reliable when the microcrystals were large enough. The same kinds of microcrystals appear at 1100 K (Fig. 6b). These are spinel (35 ± 15 nm) intermediate between magnesioferrite ($MgFe_2O_4$), ulvöspinel (Fe_2TiO_4) and hercynite ($FeAl_2O_4$), and an SiO_2-poor pyroxene (Table 5) with a mean size of 10 ± 5 nm whose composition bears some analogy with that reported by Cosca and Peacor [26] for an esseneite of ideal formula $CaFe^{3+}AlSiO_6$. More important, we emphasize that the chemical composition of the residual glass is homogeneous after crystallization. In other words, diffusion in the supercooled residual melts is sufficiently rapid to ensure re-equilibration of the system on the time scale of the viscosity experiments. Taking as the average divalent cation diffusion coefficient the values given by Cooper et al. [27] for a basaltic glass, we find that the characteristic length ($\lambda = 2\sqrt{Dt}$ where D is the diffusion coefficient and t is time) is about 2 μm at around 950 K in a 12-h experiment. This

Table 4
Tammann–Vogel–Fulcher (TVF) parameters of the three basalt samples (cf. Table 3), and average absolute deviations (AAD) of the experimental data from the fitted values

$Fe^{2+}/\Sigma Fe$	A	B	T_1	AAD
0.16	−3.46	3741	695.8	0.03
0.43	−3.59	3910	673.0	0.03
0.83	−3.48	3653	678.3	0.06

Table 5
Chemical composition (wt%) of crystalline phases

	Spinel[a]	Pyroxene[a]	Esseneite[5b]
SiO_2		27.8	29.51
Fe_2O_3			23.89
FeO	70.4	16.0	0.69
Al_2O_3	3.9	19.0	17.95
CaO		12.6	23.40
MgO	9.9	17.4	2.68
MnO			0.11
Na_2O		1.1	0.14
TiO_2	15.8	6.1	0.99

[a] Total iron expressed as FeO.
[b] Cosca and Peacor [26].

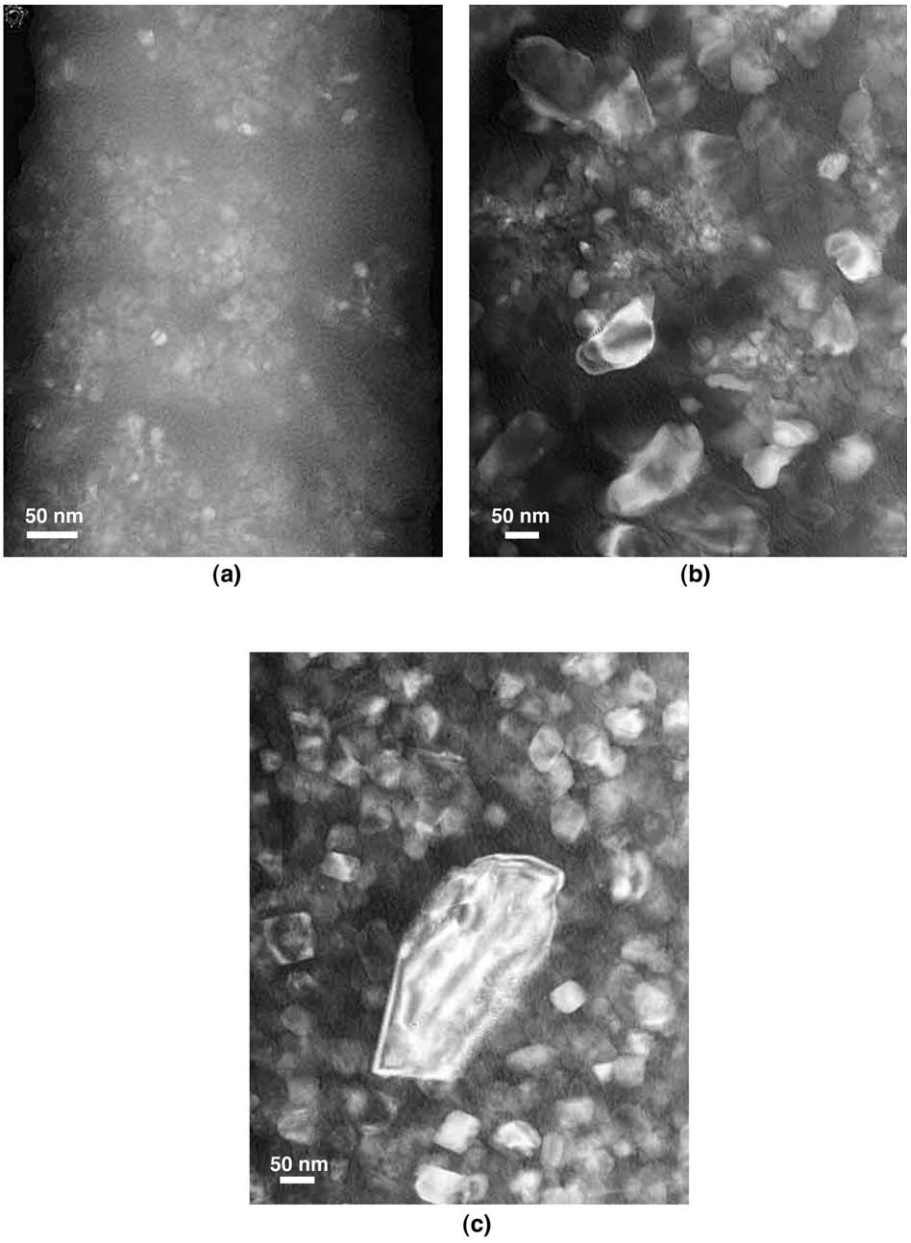

Fig. 6. TEM observations of partial crystallization of molten basalt and size increase of the crystals with increasing temperature. (a) Microcrystals of about 10 nm in the glassy matrix. (b) Phases forming near 1100 K: pyroxene (size: 10 ± 5 nm) and spinel (35 ± 15 nm). (c) Phases forming near 1300 K: pyroxene (70 ± 15 nm) and spinel (300 ± 50 nm).

length is much larger than the average distance between crystals in the partially crystallized samples after viscosity experiments (cf. Fig. 6a).

The same crystals were observed after experiments at 1200 and 1300 K. At 1200 K their size was generally smaller than 40 nm. It increases to 300 and 70 nm for spinel and pyroxene at 1300 K, respectively (Fig. 6c). Correlatively, the total crystal fraction increases. For example, the spinel and pyroxene phases represent about 1 and 40 vol% at

1100 K, respectively, and 5 and 55 vol% at 1300 K. As a result of crystallization of a silica-poor pyroxene, the composition of the residual glass matrix becomes considerably enriched in SiO_2. This variation is linear in the temperature range studied, the SiO_2 content increasing from about 47 wt% at 970 K to 60 wt% at 1100 K, and to 75 wt% at 1300 K (Table 6). These crystalline phases are similar to those observed during reheating of Kilauea basalt glasses [28,29].

Finally, for the SFB samples with $r = 0.43$ we observed after viscosity measurements made between 930 and 950 K that the crystal fraction was about 5 vol% with about 1 vol% of spinel and 4 vol% of pyroxene phases.

3.4. Non-Newtonian rheology

In static measurements, the rheology of most samples remained Newtonian once the viscosity had reached the limiting values shown in Figs. 1 and 3. The only exception is sample B5, whose viscosity was non-Newtonian in the 10–100 MPa stress range that could be investigated (Fig. 7). These relationships point to a pseudoplastic behavior, probably originating in interactions between the crystalline inclusions. They extrapolate to non-zero stresses at zero strain, which markedly decrease with increasing temperature. For sample B5, the apparent yield strength thus decreases from 20 MPa at 1121 K to 6 MPa at 1163 K. Non-Newtonian rheology was not investigated in the dynamic measurements plotted in Fig. 5 since the stress was kept constant.

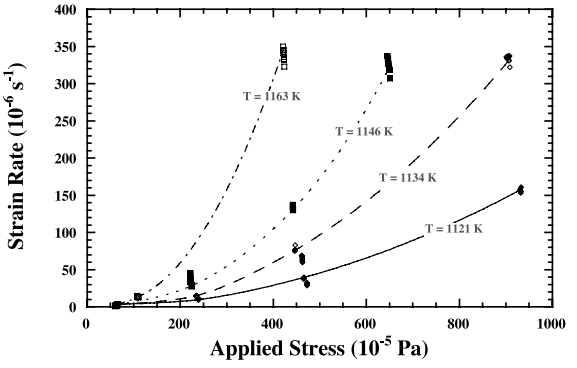

Fig. 7. Strain rate as a function of the applied stress for the SFB5 sample ($r = 0.43$) at various temperatures.

Table 6
Evolution with temperature of the chemical composition of the residual glass matrix (wt%)

	Initial	1100 K	1300 K
SiO_2	46.6	59.8	74.7
FeO[a]	11.2	7.3	1.2
Al_2O_3	13.3	9.9	4.3
CaO	10.0	5.3	2.0
MgO	9.3	4.5	1.7
Na_2O	5.6	9.0	11.9
K_2O	1.4	2.4	3.5
TiO_2	2.6	1.6	0.5

[a] Total iron expressed as FeO.

In a few additional runs, however, we did observe that the viscosity was decreasing strongly when the stress was increased above 1150 K. At 1160 K, for example, the viscosity decreased from $10^{11.44}$ to $10^{10.63}$ Pa s when the stress varied from 240 to 930 MPa. Since the effect of temperature is predominant in Fig. 7, the apparent yield strength varies more with temperature than with crystal fraction, in agreement with the conclusions drawn in previous studies of simple silicate melts under similar experimental conditions [15,16].

3.5. Physical vs. chemical effects on the viscosity of partially crystallized basalt

Additional experiments have been done to separate the physical and chemical effects on the viscosity of partially crystallized basalt and to account in a quantitative way for the former. These were low-temperature measurements of the viscosities of five melts whose composition simulates that of the residual liquid after formation of 5, 10, 20, 40 and 60 vol% of crystals as determined from chemical analyses performed with our analytical transmission electron microscope (cf. Table 1). The results are listed in Table 7 and plotted in Fig. 8 against temperature. From SFB5–SFB20, the viscosity changes are very small. For the higher silica fractions of SFB40 and SFB60, the viscosity actually decreases because of the increasing amounts of alkaline-earth and especially of alkali oxides. For extrapolation purposes, empirical TVF equations have been fitted to the high- and low-viscosity data for each composition (Table 8). The low-viscosity values

Table 7
Viscosities of synthetic glassy matrices SFB5, SFB10, SFB20, SFB40 and SFB60 (Pa s)

T (K)	log η	T (K)	log η	T (K)	log η	T (K)	log η	T (K)	log η
SFB5		SFB10		SFB20		SFB40		SFB60	
906.1	12.55	914.8	12.18	910.6	12.05	867.2	12.39	810.3	11.87
915.8	12.02	925.2	11.61	917.1	11.70	883.9	11.63	821.1	11.45
925.5	11.51	935.2	11.10	923.1	11.37	894.5	11.24	830.1	11.07
935.8	10.95	945.2	10.59	934.0	10.91	902.9	10.90	840.8	10.75
946.8	10.40	955.1	10.02	945.8	10.42	913.5	10.50	852.1	10.39
962.5	9.65	969.6	9.33	956.2	9.99	928.8	9.94	862.8	10.06
973.9	9.10	980.9	9.13[a]	966.9	9.54	944.1	9.42	872.9	9.77
994.5	8.49[a]	992.2	8.97[a]	977.5	9.10	958.8	9.02	887.3	9.37
1017.7	8.04[a]	1002.9	8.94[a]	993.2	8.48	971.4	8.66	898.4	9.05
1473	1.55	1021.5	8.44[a]	1017.0	7.78	983.7	8.33	910.4	8.76
1573	1.02	1473	1.62	1046.7	6.95	1004.9	7.82	923.9	8.42
1673	0.60	1573	1.08	1473	1.75	1473	2.31	933.6	8.22
1773	0.24	1673	0.66	1573	1.22	1573	1.75	952.4	7.89
		1773	0.29	1673	0.79	1673	1.36	966.5	7.67
				1773	0.41	1773	1.02	1473	3.07
								1573	2.51
								1673	2.07
								1773	1.68

The viscosities at 1473, 1573, 1673 and 1773 K of all compositions were calculated with the model of Bottinga and Weill [30].
[a] Indicates viscosity increase (crystallization) during measurements.

were calculated from Bottinga and Weill's [30] model (see Table 7). Interestingly, there is a viscosity cross-over near 1100 K above which the most siliceous melts become the more viscous. Although there is some scatter in the data listed in Table 8, these trends are borne out by the TVF parameters and T_{12} temperatures (T_{12} is the temperature at which the viscosity is 10^{12} Pa s). Near this temperature, where our measurements have been made, the important conclusion is thus that the viscosity increases due to crystallization cannot result from the changing composition of the residual liquid. In other words, these effects are physical in origin and result from interactions between the suspended crystals.

4. Discussion

4.1. Iron state, viscosity and partial crystallization

Consistent with previous studies [6–11,13,31], our measurements show that the viscosity of molten basalt increases when the starting material becomes more oxidized. The effect of the redox state on viscosity is more pronounced at lower than at higher temperatures. As an example, the difference between the viscosities of oxidized and reduced basalt melts is about 1.5 and 0.3 log-units at 950 and 1400 K, respectively. Since the glass transition temperature is operationally defined as the temperature at which the viscosity is 10^{12} Pa s, it also depends on the redox state of the melt. From the parameters of Table 3, T_{12} is about 940, 925 and 915 K for $Fe^{2+}/\Sigma Fe = 0.16$, 0.43 and 0.83, respectively, thus decreasing with increasing $Fe^{2+}/\Sigma Fe$ ratio (Fig. 9). Such trends are generally interpreted to mean that Fe^{3+} is essentially a network former and Fe^{2+} a network modifier [32], so that oxidation of Fe^{2+} to Fe^{3+} results in changes in the degree of polymerization and hence in the viscosity.

With regard to the effects of crystallization on viscosity, we first note that their magnitude increases markedly with the iron content of the melt. At about the same viscosities, increases of only an order of magnitude have been observed for andesite liquids with about 5 wt% total FeO

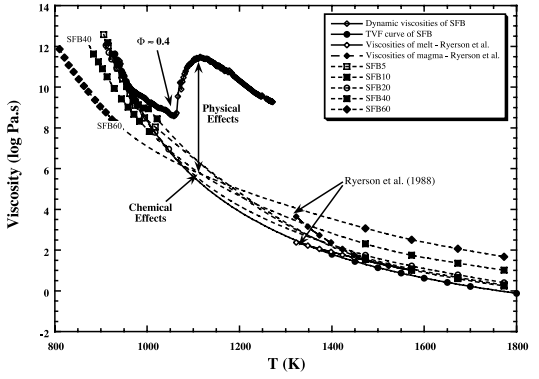

Fig. 8. Viscosities of liquid matrix compositions measured isothermally at low temperatures and calculated at high temperatures with Bottinga and Weill's [30] model. For comparison, the TVF and dynamic curves of SFB ($r = 0.43$), and the data at high temperatures of Ryerson et al. [18] for another basalt composition are reported.

[14,33] and of half an order of magnitude for a molten rhyolite with 0.8 wt% total FeO [14]. The kinetics of crystal nucleation/growth strongly depend on the iron state, increasing with an increasing proportion of Fe^{3+}. Although the compositional changes of the liquid matrix are essentially due to the growth of pyroxene, the first phase to nucleate homogeneously is a spinel. The pyroxene then nucleates heterogeneously, as has been described for a variety of supercooled liquids in the system FeO–CaO–MgO–Al_2O_3–SiO_2 [6,34–37].

The volume fraction of spinel has been observed to decrease with decreasing oxygen fugacity [35]. In view of pyroxene nucleation on spinel, this is probably why basalt melts crystallize much faster under oxidizing than under reducing conditions [6,38,39]. These observations are thus consistent with our measurements, which clearly show the influence of iron on basalt crystallization and that the presence of iron in the form of Fe^{3+} is essential for the viscosity to increase with time.

In view of the crystal fractions reported in the preceding section, our observations are consistent with the rheological changes observed for the two simple systems, namely $Mg_3Al_2Si_3O_{12}$ [15] and $Ca_2Al_2Si_2O_8$ melts [16]. In both studies, a transition from Newtonian to non-Newtonian rheology was observed for crystal fractions of 30–40 vol%, at which the inclusions begin to interact. The transition is slightly less abrupt for crystals having different shapes and showing a size distribution investigated by Lévesque et al. [16] than for the spherical particles of nearly the same size studied by Lejeune and Richet [15]. The rheological transition that takes place in crystallizing basalt melts should thus be more similar to the former case. There exists an important difference with these results, however, in that the observed increases of Newtonian viscosities remained lower than one order of magnitude because congruent crystallization left the melt composition unchanged in the later studies [15,16].

Table 8
Tammann–Vogel–Fulcher (TVF) parameters of synthetic glassy matrices SFB5, SFB10, SFB20, SFB40 and SFB60, and temperature at which the viscosity is 10^{12} Pa s (T_{12})

	A	B	T_1	AAD[a]	T_{12} (K)
SFB5	−3.26	3900	660.4	0.04	916
SFB10	−3.03	3691	672.8	0.04	918
SFB20	−3.34	4273	633.5	0.04	912
SFB40	−3.15	5106	539.0	0.02	876
SFB60	−1.82	4761	461.6	0.06	806

[a] Average absolute deviation of the experimental data from the fitted values.

4.2. *Prediction of the viscosity of partially crystallized melts*

The composition dependence of viscosity has a considerable geochemical and industrial impor-

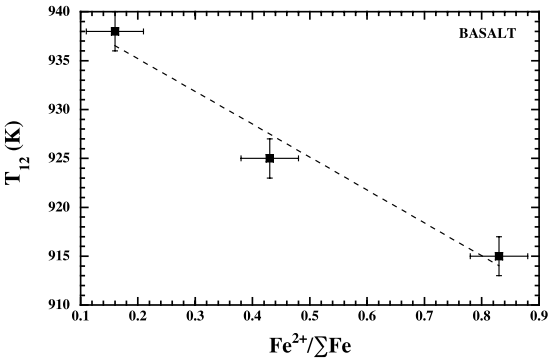

Fig. 9. Variation of T_{12} against the redox ratio $Fe^{2+}/\Sigma Fe$.

tance. Quantitative predictions of viscosity as a function of composition and temperature over wide ranges of temperature and composition remain difficult, however, because of the complexity of the variations of viscosity especially near the glass transition. Covering a wider temperature range than the classical model of Bottinga and Weill [30] for superliquidus temperatures, the recent model of Giordano and Dingwell ([40] and personal communication), for instance, reproduces the viscosity data of Tables 2 and 7 reasonably well in its interval of calibration. Except for samples SFB40 and SFB60, the model of Giordano and Dingwell reproduces all the other viscosities to within one order of magnitude; this is essentially due to the extremely high peralkalinity of these samples.

To make more precise predictions, essentially around the glass transition temperature, we have followed an approach similar to that of Williams et al. [41] and Taniguchi [42]. The viscosity in this case can be expressed by the following equation:

$$\log(\eta/\eta_{T_{12}}) = A(T-T_{12})/[B+(T-T_{12})] \quad (3)$$

where η is the viscosity in Pa s, T_{12} the temperature at which the viscosity is 10^{12} Pa s, and A and B are constants independent of chemical composition. In fact, expressions like Eq. 3 implicitly incorporate the effects of composition through the parameter T_{12} of the homogeneous composition. In this work, we determined the constants A and B by fitting the viscosity data of several compositions as a function of $(T-T_{12})$ and observing that a single master curve can be obtained with the parameters $A=-15.7$ and $B=285$ K (Fig. 10). These values are similar to those found by Taniguchi [42] for melts along the diopside–anorthite join. The viscosity data used in our fit are those of Sipp et al. [43] (NC and BNC compositions), some titanosilicate melts [44] and the data for diopside, Mg76.11 and Ca76.11 samples [45]. Although there is some scatter in the data, no systematic deviation due to compositional change is observed and the deviations from the model values are lower than half an order of magnitude at low temperatures and lower than one order of magnitude at higher temperatures.

With Eq. 3 and the parameters A and B found in this work one can reproduce the viscosity data of Tables 2 and 7 to better than 0.4 order of magnitude near the glass transition temperatures, and to within 0.5 order of magnitude at higher temperatures for all compositions, except SFB60 for which the difference is twice as great near the glass transition temperature. This equation could thus be used, at least for other basic melts, provided that the temperature T_{12} is known.

Beginning with Einstein's work, several studies have been devoted to the prediction of the viscosity of partially crystallized liquids. The Einstein–Roscoe equation is the most widely used by using the following equation:

$$\eta = \eta_0(1-\Phi/\Phi_m)^{-n} \quad (4)$$

where η_0 is the viscosity of the homogeneous melt, Φ is the crystal fraction and Φ_m and n are adjustable parameters that have been extensively used to account for the viscosity of partially crystallized melts (e.g. [15,18,46–48]). Different sets of n and Φ_m parameters have been suggested by these authors. The values of Φ_m depend not only on the size, but also on the shape and size distribution of the particles in the melt. As an example, Φ_m ranges from 0.74 to 0.6 for suspended spheres of equal size, depending on the packing density. As Φ_m and n are strongly correlated, values of n ranging from 1.5 to 5 have been proposed.

Our results do not allow us to suggest appro-

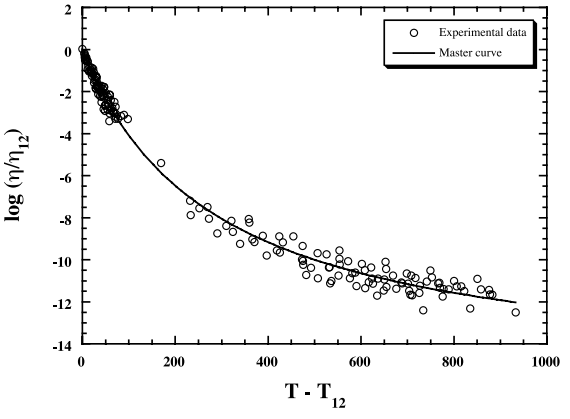

Fig. 10. Viscosities of several compositions and the derived unified curve with $A=-15.7$ and $B=285$ (Eq. 3, see text).

priate values for these parameters because we did not determine accurately any viscosity–crystal fraction relationship. We just note that, with the standard values $n = 2.5$ and $\Phi_m = 0.75$, the viscosity increases plotted in Fig. 1 are accounted for if one takes a crystal fraction of about 5 vol% at the end of the measurements, as suggested by TEM observations. As long as the viscosity does not depart markedly from Newtonian behavior, we thus conclude that Eqs. 3 and 4 provide a reasonable description of the viscosity of partially crystallizing basalts.

At higher crystal fractions the effects of course become more important and more complex since the viscosity of the suspension can vary by orders of magnitude depending on the stress applied. For a constant stress of around 9×10^7 Pa, the relative importance of physical and chemical effects can be determined from the differences shown in Fig. 8 between the viscosities of the partially crystallized samples and residual liquids. Of particular importance is the rapid viscosity increase observed for a crystal fraction of about 40 vol%. This is consistent with the observations made on simpler, congruently crystallizing systems [15,16]. We have also plotted in Fig. 8 the high-temperature observations made by Ryerson et al. [18] on another basalt up to a crystal fraction of 69 vol% at the lowest temperature investigated of 1323 K. Because the viscosity is markedly non-Newtonian at such high crystal fractions, comparisons between both kinds of measurements are impossible. The trends observed in both studies are nevertheless mutually consistent.

Acknowledgements

We thank S. Vignesoult for his interest in this work, donating samples and making available to us high-temperature viscometry, B.O. Mysen for Mössbauer analyses and A. Sipp, A. Whittington and V. Magnien for fruitful advice at various stages of this study. We thank B.O. Mysen, D.B. Dingwell and an anonymous reviewer for their helpful comments. Work supported in part by the E.U. Project ENV4-CT98-0713 'Parametrisation and Modelling of Lava Flows'. *[BW]*

References

[1] H.R. Shaw, Rheology of basalt in the melting range, J. Petrol. 10 (1969) 510–535.
[2] T. Murase, A.R. McBirney, Properties of some common igneous rocks and their melts at high temperatures, Geol. Soc. Am. Bull. 84 (1973) 3563–3592.
[3] M. Cukierman, D.R. Uhlmann, Effects of iron oxidation state on viscosity, Lunar Composition 15555, J. Geophys. Res. 79 (1974) 1594–1598.
[4] P. Exnar, J. Voldan, Measuring viscosity with the penetration viscometer, Silikaty 26 (1982) 251–259.
[5] D. Giordano, D.B. Dingwell, Viscosity of hydrous Etna basalt: implications for Plinian-style basaltic eruptions, Bull. Volcanol. 65 (2003) 8–14.
[6] J. Williamson, A.J. Tipple, P.S. Rogers, Influence of iron oxides on kinetics of crystal growth in CaO-MgO-Al_2O_3-SiO_2 glasses, J. Iron Steel. Inst. 206 (1968) 898–903.
[7] L.C. Klein, B.V. Fasano, J.M. Wu, Flow behavior of ten iron-containing silicate compositions, Proc. Lunar Planet. Sci. 12B (1981) 1759–1767.
[8] L.C. Klein, B.V. Fasano, J.M. Wu, Viscous flow behavior of four iron-containing silicates with alumina, effects of composition and oxidation condition, J. Geophys. Res. 88 (1983) A880–A886.
[9] G. Urbain, Y. Bottinga, P. Richet, Viscosity of liquid silica, silicates and alumino-silicates, Geochim. Cosmochim. Acta 46 (1982) 1061–1072.
[10] A. Montenero, M. Friggeri, D.C. Giori, N. Belkhiria, L.D. Pye, Iron-soda-silica glasses: preparation, properties, structure, J. Non-Crystal. Solids 84 (1986) 45–60.
[11] D.B. Dingwell, D. Virgo, The effect of oxidation state on the viscosity of melts in the system Na_2O-FeO-Fe_2O_3-SiO_2, Geochim. Cosmochim. Acta 51 (1987) 195–205.
[12] D.B. Dingwell, D. Virgo, Viscosities of melts in the Na_2O-FeO-Fe_2O_3-SiO_2 system and factors controlling the relative viscosities of fully polymerized silicate melts, Geochim. Cosmochim. Acta 52 (1988) 395–403.
[13] D.B. Dingwell, Redox viscometry of some Fe-bearing silicate melts, Am. Mineral. 76 (1991) 1560–1562.
[14] D.R. Neuville, P. Courtial, D.B. Dingwell, P. Richet, Thermodynamic and rheological properties of rhyolite and andesite melts, Contrib. Mineral. Petrol. 113 (1993) 572–581.
[15] A.M. Lejeune, P. Richet, Rheology of crystal-bearing silicate melts: An experimental study at high viscosities, J. Geophys. Res. 100 (B3) (1995) 4215–4229.
[16] S. Lévesque, P. Richet, D.R. Neuville, Rheology and crystallization of magmas: $CaAl_2Si_2O_8$ melt as a model system, J. Geophys. Res. (2003) to be submitted.
[17] H. Pinkerton, R.S.J. Sparks, Field measurements of the rheology of lavas, Nature 276 (1978) 383–385.
[18] F.J. Ryerson, H.C. Weed, A.J. Piwinskii, Rheology of subliquidus magmas 1. Picritic compositions, J. Geophys. Res. 93 (1988) 3421–3436.
[19] H. Pinkerton, G. Norton, Rheological properties of basaltic lavas at sub-liquidus temperatures: laboratory and

field measurements on lavas from Mount Etna, J. Volcanol. Geotherm. Res. 68 (1995) 307–323.
[20] J.F. Schairer, N.L. Bowen, The system K_2O-Al_2O_3-SiO_2, Am. J. Sci. 253 (1955) 681–746.
[21] D.R. Neuville, P. Richet, Viscosity and mixing in molten (Ca, Mg) pyroxenes and garnets, Geochim. Cosmochim. Acta 55 (1991) 1011–1019.
[22] S. Vignesoult, S. Thelohan, Influence of iron content and redox level on physical properties of glasses, in: Fundamentals of Glass Science and Technology, ESG, Venice, 1993, pp. 643–646.
[23] E. Van Cappellen, The parameterless correction method in X-ray microanalysis, Microsc. Microanal. Microstruct. 1 (1990) 1–22.
[24] E. Van Cappellen, J.C. Doukhan, Quantitative transmission X-ray microanalysis of ionic compounds, Ultramicroscopy 53 (1994) 343–349.
[25] D. Bouchet, J. Ingrin, Report on the 1993 and 1994 round robin EDXS tests of the Ile de France TEM network, Microsc. Microanal. Microstruct. 6 (1995) 385–392.
[26] M.A. Cosca, D.R. Peacor, Chemistry and structure of esseneite ($CaFe^{3+}AlSiO_6$), a new pyroxene produced by pyrometamorphism, Am. Mineral. 72 (1987) 148–156.
[27] R.F. Cooper, J.B. Fanselow, D.B. Poker, The mechanism of oxidation of a basaltic glass: chemical diffusion of network-modifying cations, Geochim. Cosmochim. Acta 60 (1996) 3253–3265.
[28] D.J.M. Burkhard, Crystallization and oxidation of Kilauea basalt glass: processes during reheating experiments, J. Petrol. 42 (2001) 507–527.
[29] D.J.M. Burkhard, Kinetics of crystallization: example of micro-crystallization in basalt lava, Contrib. Mineral. Petrol. 142 (2002) 724–737.
[30] Y. Bottinga, D. Weill, The viscosity of magmatic silicate liquids: a model for calculation, Am. J. Sci. 272 (1972) 438–475.
[31] C. Liebske, H. Behrens, F. Holtz, R.A. Lange, The influence of pressure and composition on the viscosity of andesitic melts, Geochim. Cosmochim. Acta 67 (2003) 473–485.
[32] B.O. Mysen, Magmatic silicate melts: Relations between bulk composition, structure, and properties, in: B.O. Mysen (Ed.), Magmatic Processes: Physicochemical Principles, Geochemical Society, University Park, PA, 1987.
[33] P. Richet, A.M. Lejeune, F. Holtz, J. Roux, Water and the viscosity of andesite melts, Chem. Geol. 128 (1996) 185–197.
[34] P.S. Rogers, J. Williamson, The nucleation of crystalline phases in silicate glasses containing iron oxides, Glass Technol. 10 (1969) 128–133.
[35] R. Hill, P. Roeder, The crystallization of spinel from basaltic liquid as a function of oxygen fugacity, J. Geol. 82 (1974) 709–729.
[36] G.H. Beall, H.L. Rittler, Basalt glass ceramics, Bull. Am. Ceram. Soc. 55 (1976) 579–582.
[37] G.B. Cook, R.F. Cooper, T. Wu, Chemical diffusion and crystalline nucleation during oxidation of ferrous iron-bearing magnesium aluminosilicate glass, J. Non-Cryst. Solids 120 (1990) 207–222.
[38] E.F. Osborn, Role of oxygen pressure in the crystallization and differentiation of basaltic magma, Am. J. Sci. 257 (1959) 609–647.
[39] J.M. Duke, The effect of oxidation on the crystallization of an alkali basalt from the Azores, J. Geol. 82 (1974) 524–528.
[40] D. Giordano, D.B. Dingwell, Non-Arrhenian multicomponent melt viscosity: a model, Earth Planet. Sci. Lett. 208 (2003) 337–349.
[41] M.L. Williams, R.F. Landel, J.D. Ferry, The temperature dependence of relaxation mechanisms in amorphous polymers and other glass-forming liquids, J. Am. Chem. Soc. 77 (1955) 3701–3707.
[42] H. Taniguchi, Universal viscosity-equation for silicate melts over wide temperature and pressure ranges, J. Volcanol. Geotherm. Res. 66 (1995) 1–8.
[43] A. Sipp, D.R. Neuville, P. Richet, Viscosity, configurational entropy and relaxation kinetics of borosilicate melts, J. Non-Cryst. Solids 211 (1997) 281–293.
[44] M.A. Bouhifd, A. Sipp, P. Richet, Heat capacity, viscosity, and configurational entropy of alkali titanosilicate melts, Geochim. Cosmochim. Acta 63 (1999) 2429–2437.
[45] A. Sipp, Propriétés de relaxation des silicates vitreux et fondus, Thesis, University Paris VII, 1998, 231 pp.
[46] J.S. Chong, E.B. Christiansen, A.D. Baer, Rheology of concentrated suspensions, J. Appl. Polymer Sci. 15 (1971) 2007–2021.
[47] A.R. McBirney, T. Murase, Rheological properties of magmas, Annu. Rev. Earth Planet. Sci. 13 (1984) 337–357.
[48] H. Pinkerton, R.J. Stevenson, Methods of determining the rheological properties of magmas at subliquidus temperatures, J. Volcanol. Geotherm. Res. 53 (1992) 47–66.